In vivo, Noninvasive, Label-Free Detection and Eradication of Circulating Metastatic Melanoma Cells Using Two-Color Photoacoustic Flow Cytometry with a Diode Laser

Ekaterina I. Galanzha,[1,2] Evgeny V. Shashkov,[1] Paul M. Spring,[2] James Y. Suen,[2] and Vladimir P. Zharov[1,2]

[1]Phillips Classic Laser and Nanomedicine Laboratories, [2]Department of Otolaryngology-Head and Neck Surgery, University of Arkansas for Medical Sciences, Little Rock, Arkansas

Abstract

The circulating tumor cell (CTC) count has been shown as a prognostic marker for metastasis development. However, its clinical utility for metastasis prevention remains unclear, because metastases may already be present at the time of initial diagnosis with existing assays. Their sensitivity *ex vivo* is limited by a small blood sample volume, whereas *in vivo* examination of larger blood volumes may be clinically restricted by the toxicity of labels used for targeting of CTCs. We introduce a method for *in vivo* photoacoustic blood cancer testing with a high-pulse-repetition-rate diode laser that, when applied to melanoma, is free of this limitation. It uses the overexpression of melanin clusters as intrinsic, spectrally-specific cancer markers and signal amplifiers, thus providing higher photoacoustic contrast of melanoma cells compared with a blood background. In tumor-bearing mouse models and melanoma-spiked human blood samples, we showed a sensitivity level of 1 CTC/mL with the potential to improve this sensitivity 10^3-fold in humans *in vivo*, which is impossible with existing assays. Additional advances of this platform include decreased background signals from blood through changes in its oxygenation, osmolarity, and hematocrit within physiologic norms, assessment of CTCs in deep vessels, *in vivo* CTC enrichment, and photoacoustic-guided photothermal ablation of CTCs in the bloodstream. These advances make feasible the early diagnosis of melanoma during the initial parallel progression of primary tumor and CTCs, and laser blood purging using noninvasive or hemodialysis-like schematics for the prevention of metastasis. [Cancer Res 2009;69(20):7926–34]

Introduction

Most cancer deaths are a result of metastatic spread of the primary tumor (1). Detection of circulating tumor cells (CTCs) seems to be a marker for metastasis development, cancer recurrence, and therapeutic efficacy (2). However, incurable metastases can develop by the time of initial diagnosis with existing CTC assays, in which sensitivity (1–5 CTC/mL) is limited by the small (5–10 mL) blood volume (3, 4). The sensitivity can be improved by assessment of a significantly larger blood volume *in vivo*, potentially the patient's entire blood volume (in adults ~5 liters; refs. 5–7). Due to the low endogenous contrasts of most cancer cells, the fluorescent labeling of CTCs *in vivo* was applied, which raises practical concerns regarding the toxicity of tags, undesired immune responses, as well as light scattering and autofluorescence background allowing the assessment of only superficial blood microvessels with a slow flows (5, 7). As an alternative, photoacoustic imaging using endogenous chromophores (e.g., hemoglobin or melanin) or exogenous nanoparticles as photoacoustic contrast agents provides higher spatial resolution in deeper tissue compared with most optical modalities (8–10). Applied to a study for melanoma, photoacoustic techniques have shown promise for assessment of melanoma cells *in vitro* (11, 12) and imaging of melanoma tumor *in vivo* in static conditions (9). However, dynamic detection of circulating melanoma cells *in vivo* has not yet been reported. Recently, we have developed time-resolved photoacoustic flow cytometry (PAFC) and showed its potential for *in vivo* real-time detection of circulating squamous cell carcinoma cells labeled with gold nanorods (GNR) and nonlabeled melanoma cells in relatively slow lymph flow (6, 13, 14). However, a low laser pulse rate prevented the detection of every CTC within fast-flowing blood. Based on a new advanced PAFC schematic with a high pulse-repetition-rate diode laser, here, we show an ultrasensitive, label-free, photoacoustic enumeration of melanoma CTCs in the blood circulation that can be integrated with simultaneous laser ablation.

Materials and Methods

Cells. HTB-65 and MALME-3M human melanoma cells, and B16F10 mouse melanoma cells were obtained directly from a cell bank (American Type Culture Collection) for 1 to 3 mo before experiments. Cells were cultured using standard procedures, including serial passage in phenol-free RPMI 1640 (Invitrogen) supplemented with 10% fetal bovine serum (Invitrogen). CD9151 and CE9151 cells were grown in Tyr-HRAS+ Ink4a/Arf−/− transgenic mice, which were characterized histologically as amelanotic (15).

Animals. According to University of Arkansas for Medical Sciences Institutional Animal Care and Use Committee–approved protocols, the experiment involved a nude mouse model. The estimation of the influence of skin melanin on detection limits was preformed with Harlan-Sprague mice, strain NIH-BG-NU-XID, with high skin pigmentation. After administration of standard anesthesia (ketamine/xylazine, 50/10 mg/kg, i.p.), animals were placed on the heated microscope stage with a topical application of warm water for acoustic matching of the ultrasound transducer and the tissue. The positions of blood vessels were verified using a high-resolution optical microscopy and ultrasound technique (Vevo 770, VisualSonic, Inc.). S.c. inoculation of 10^6 B16F10 mouse melanoma cells in a 50-μL suspension provided the mouse melanoma tumor in ear and skin on the mouse. Microscopic and H&E pathologic examination and immunohistochemistry were carried out by a veterinary pathologist. The reverse

Note: Supplementary data for this article are available at Cancer Research Online (http://cancerres.aacrjournals.org/).

Requests for reprints: Vladimir P. Zharov, University of Arkansas for Medical Sciences, 4301 West Markham Street, Slot 543, Little Rock, AR 72205. Phone 501-603-1213; Fax: 501-686-8029; E-mail: zharovvladimirp@uams.edu.

doi:10.1158/0008-5472.CAN-08-4900

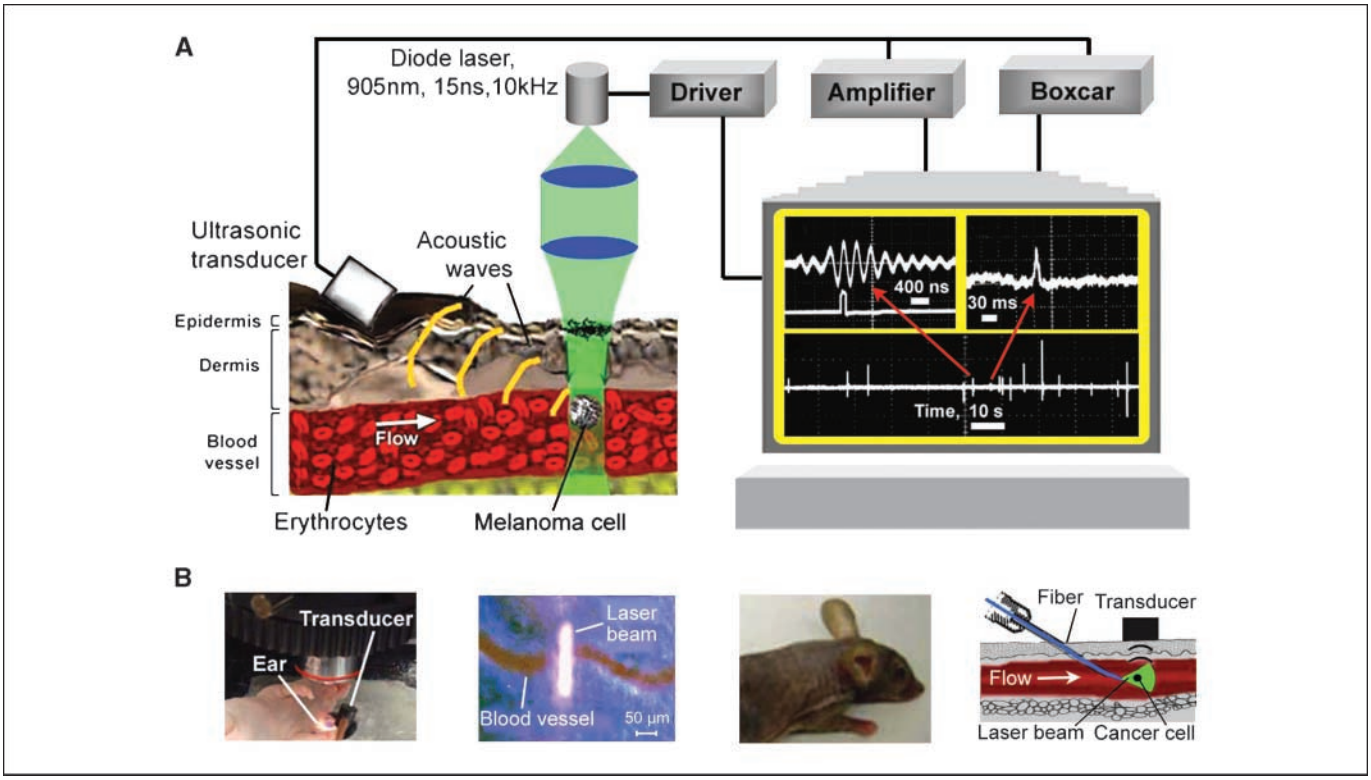

Figure 1. *A,* PAFC schematics with acquisition algorithm of photoacoustic signals. Laser parameters: 905 nm, 30 mJ/cm^2. *B,* animal models (from left to right): microscopic schematic, diode laser beam after passing of mouse ear, pigmented mouse NIH-BG-NU-XID, and minimally invasive fiber delivery of laser radiation into blood vessel.

transcription-PCR (RT-PCR) testing of blood samples from mice was provided by the National Center for Toxicological Research (Jefferson, AR).

Human blood. Fresh blood was obtained from healthy donors in heparinized tubes and added to different numbers of HTB-65 cells under the auspices of an Institutional Review Board–approved protocol at University of Arkansas for Medical Sciences; necessary informed consents were obtained from all subjects.

Nanoparticles. Melanin nanoparticles at 100 ± 30 nm (Sigma-Aldrich) were used for PAFC calibration at a concentration of ~2 μg/mL in suspension. GNRs with sizes of 15 × 50 nm and maximum absorption near 850 nm were provided by the laboratory of Nanoscale Biosensors at the Institute of Biochemistry and Physiology of Plants and Microorganisms (16). Melanoma cells were labeled by GNRs through endocytotic effects *in vitro* at 37°C for 1 h.

Experimental setup. The PAFC was built on the platform of an Olympus BX51 microscope (Olympus America, Inc.), a tunable optical parametric oscillator (OPO; wavelength of 420–2,300 nm; 8-ns pulse width; a repetition rate of 10–50 Hz; pulse fluence, 0.01–100 J/cm^2; Lotis Ltd.), and a diode laser (905 nm, 15 ns, 10 kHz, 0.01–0.7 J/cm^2, model 905-FD1S3J08S, Frankfurt Laser Company) with driver IL30C (Power Technology Inc). Photoacoustic signals were detected using an unfocused ultrasound transducer (model 6528101, 3.5 MHz, 5.5 mm in diameter; Imasonic, Inc.); or a focused cylindrical transducer (V316-SM, 20 MHz, focal length, 12.5 mm; Panametrics-NDT, Olympus) and amplifier (5660B, 2 MHz, gain 60 dB and 5678, 40 MHz, gain 60 dB, respectively; both from Panametrics- NDT, Olympus), and were recorded using a Boxcar (SR250, Stanford Research Systems, Inc.), Tektronix TDS 3032B oscilloscope, and a computer. PAFC was integrated with PT technique and transmission digital microscopy (TDM), which are described elsewhere (Supplementary Fig. S1; refs. 17–19). Briefly, in PT imaging (PTI) mode, laser-induced temperature-dependent variations in the refractive index around melanin nanoparticles were visualized with a phase-contrast technique using a second, collinear laser pulse from a Raman shifter (639 nm, 12 ns; 10–50 Hz, 0.1–2 mJ/cm^2) with a tunable delay (0–10 μs) and a CCD camera (AE-260E, Apogee Inc.; ref. 17). The pump and the probe beams have stable, Gaussian intensity profiles and adjustable diameters in the range of 10 to 40 μm and 10 to 25 μm. The resolution was determined by the microscope objective [e.g., 0.7 μm at 20×, numerical aperture (NA) 0.4; 300 nm at 60×; NA, 1.25]. In second, PT thermolens mode, a pump laser–induced refractive heterogeneity caused defocusing of a collinear He-Ne laser probe beam (wavelength, 633 nm; power, 1.4 mW), and hence, a reduction in the beam's intensity at its center detected by a photodiode (C5658; Hamamatsu Corp.) with a pinhole as PT response from a whole cell (17). The time-resolved, two-wavelength spectral identification of melanoma CTCs was realized with two laser pulses at wavelength of 865 nm (OPO) and 639 nm (Raman shifter) with 10-μs delay. An *in vitro* study was performed with cells in suspension on conventional microscope slides with 120-μm width.

Scanning TDM/PT cytometer *in vitro*. The presence of melanoma cells in the blood circulation was verified *ex vivo* by analyzing stabilized blood samples (0.5–2 mL) in a chamber (S-24737, Molecular Probes). The scanning was performed using an automatic microscopic stage (Conix Research, Inc.).

Statistical analysis. A minimum of three animals were used for each experiment unless otherwise noted. Results are expressed as means ± SEM of at least three independent experiments. Spearman correlations for which P values of <0.05 were considered statistically significant. Statistica 5.11 (StatSoft, Inc.), MATLAB 7.0.1 (MathWorks), and *LabVIEW* (National Instruments) were used for the statistical calculations.

Results

PAFC schematic. The photoacoustic detection of melanoma CTCs was based on transformation of absorbed energy in melanin nanoparticles into heat accompanied by thermal nanoparticle expansion leading to the generation of acoustic waves (Fig. 1*A*). To

expose each CTC, the laser pulse repetition rate, f, was adjusted as $f \geq V_F/2R_{CTC}$, where V_F is the flow velocity, and R_{CTC} is the radius of CTCs (13). In peripheral microvessels with diameter of 10 to 70 μm, the flow velocity ranged from 1 mm/s (capillary) to 10 mm/s (arterioles; refs. 20, 21), and for R_{CTC} = 10 μm, $f \geq$50, 500 Hz, respectively. We integrated a previously described PAFC (13) with a high pulse rate (10 kHz) diode laser (905 nm), which provided a linear beam configuration on skin with a size of 11 μm × 75 μm (Fig. 1*B*). The photoacoustic signal from a single CTC had an initial bipolar shape that transformed into a pulse train due to resonance and reflections effects in the transducer-skin-holder interface (Fig. 1*A, left top trace*). Because of the short duration (~5–10 μs), the compressed signals appeared as vertical lines (Fig. 1*A, bottom trace*). Control trace without CTCs is shown at the bottom of the tracing panel in Fig. 1*A*. Several (20–50) photoacoustic signals from the same CTC were acquired using Boxcar gating (Fig. 1*A, bottom on left top trace*) and transformed into unipolar signals with a width determined by the transit time of the CTC through the laser beam (Fig. 1*A, right top trace*). From the full width at half maximum of 10 ms and the average beam diameter of 35 μm, the flow of velocity was estimated as ~3.5 mm/s for a 50-μm ear vein, which is in agreement with the available data (5, 7).

To estimate the variable expression of melanin in tumor cells (15, 22–25), we measured the PT thermolens signals and PT image structures as indicators of average melanin content and melanin spatial distribution in individual cells, respectively. Conventional TDM provided a melanin distribution for highly pigmented cells (Supplementary Fig. S2; Fig. 2*A*). PT imaging mode with its much higher (enhancement gain, $\geq 10^4$) absorption sensitivity provided visualization of melanin nanoparticles that were invisible with TDM (Fig. 2*A*). The temporal dynamics of local structures in PT images at different time delays provides information of nanoparticle average

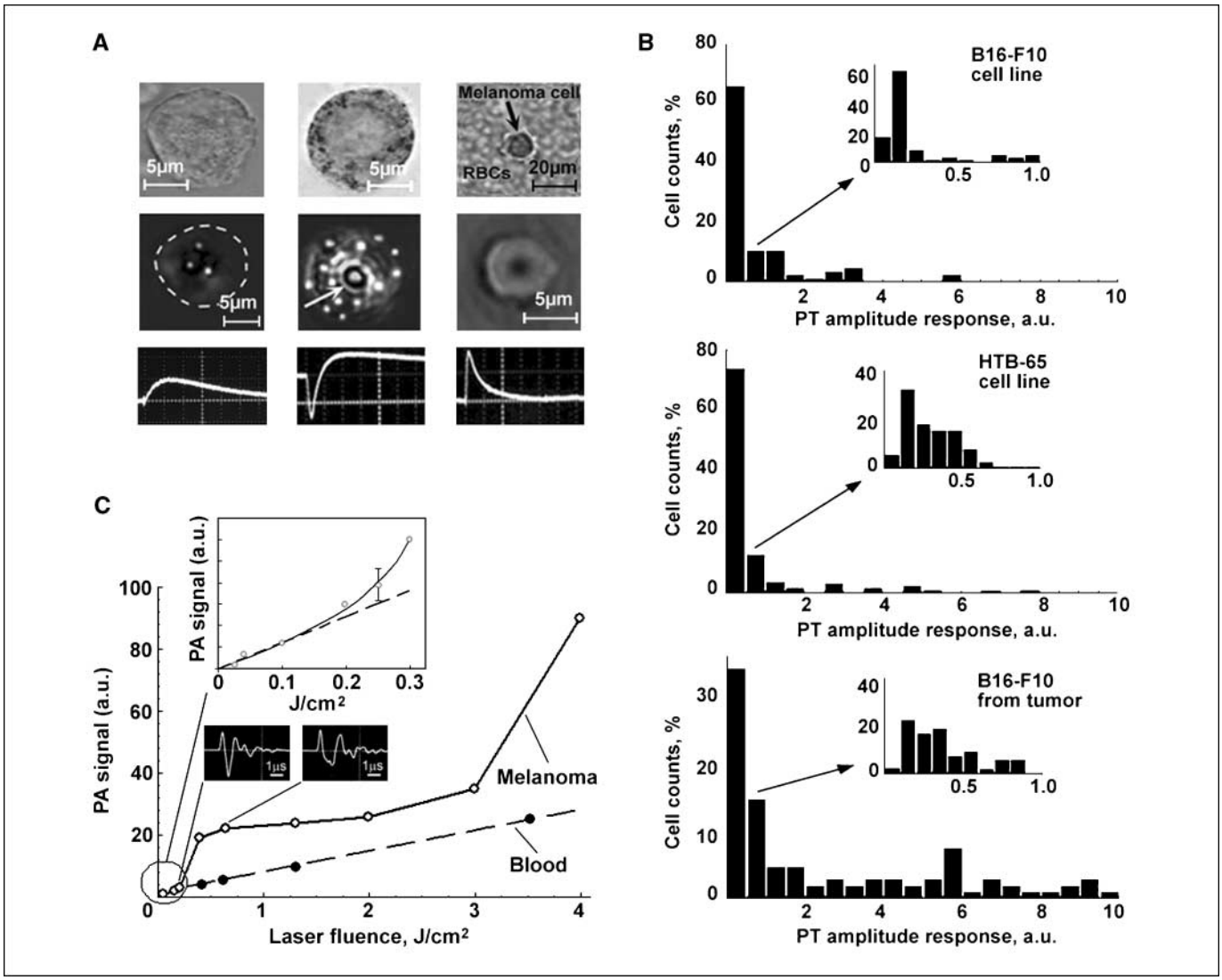

Figure 2. *A,* high-resolution (×100) TDM images of single B16F10 cells with low and high melanin content and single B16F10 cell surrounded by mouse RBCs (*first row from left to right*, respectively). PT images of B16F10 cells with low and high melanin content and single mouse RBC (*second row*, respectively). PT signals from single low and high pigmented melanoma cells and single RBC (*third row*, respectively); amplitude/time scale/laser wavelength/fluence: (20 mV/div)/(4 μs/div)/580 nm/(60 mJ/cm^2), (100 mV/div)/(4 μs/div)/580 nm/(0.3 J/cm^2), and (10 mV/div)/(4 μs/div)/580 nm/(100 mJ/cm^2), respectively. *B,* heterogeneity of the PT signal amplitudes for melanoma cells (850 nm; 0.1 J/cm^2). *Inset,* distribution details for relatively low signals. *C,* photoacoustic signals from tumor-derived B16F16 cells in suspension (10^7cell/mL) and mouse RBCs in microscopic slide with attached transducer as function of laser fluence (wavelength, 800 nm; beam diameter, 100 μm, ~60 melanoma cells and ~4 × 10^4 RBCs in the irradiated volume).

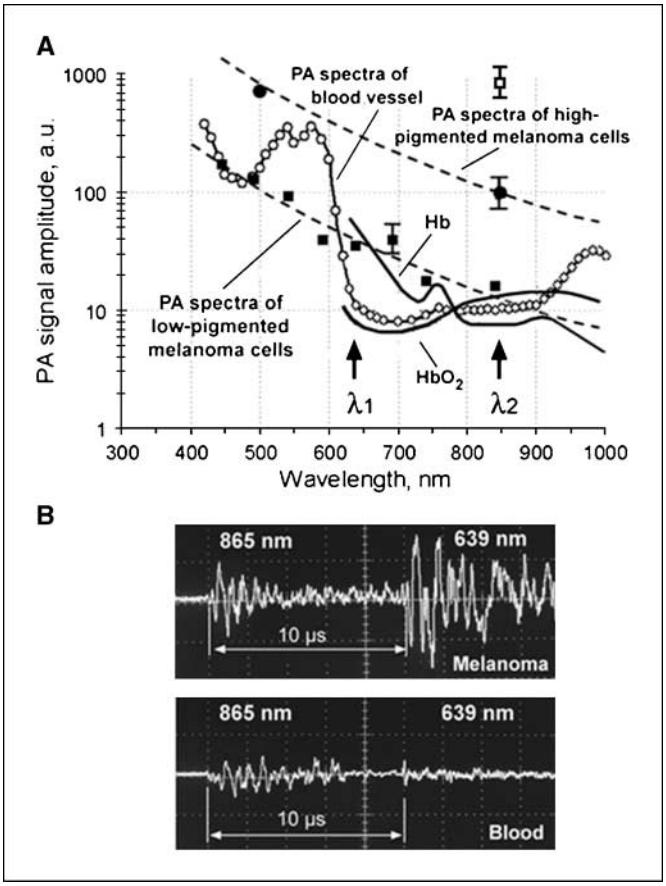

Figure 3. *A,* photoacoustic spectra of ~50 μm diameter veins in mouse ear (○); the average SEM for each wavelength is 20%. The absorption spectra of the B16F10 cells (*dashed curves*) were normalized to photoacoustic signals from single melanoma cells with strong (●) and weak (■) pigmentation; □, signal from melanoma cell with GNRs; fragment of solid curves shows absorption for 100% of Hb and HbO_2. *B,* two-wavelengths (λ_1 = 639 nm; λ_2 = 865 nm) identification of melanoma cells and RBCs.

sizes, as previously described (17). The PT thermolens signal from single cell exhibited a fast-rising (ns scale) peak associated with cell heating resulting from the averaging of thermal effects from individual melanin nanoparticles, and a slower decay (μs scale) due to cell cooling as a whole (Fig. 2*A*, *bottom*). Most melanoma cells contained scattered individual 30 to 50 nm melanin nanoparticles and nanoparticle clusters in individual melanosomes with an average diameter of 0.75 ± 0.25 μm.

Monitoring of the PT signals from individual cells (total 500) in suspension showed a high level of heterogeneity: the 5% to 10% of cells with increased pigmentation produced PT signals with an amplitude much greater than that of PT signals from cells with less pigmentation (Supplementary Fig. S2; Fig. 2*B*). The average melanin content increased in the following sequence: cultured B16F10 mouse cells–cultured HTB-65 human cells–B16F10 cells derived from primary tumor. Approximately 92 ± 3.9% of tumor-derived B16F10 cells were detectable with the PT/photoacoustic technique, compared with 87 ± 3.5% of the HTB-65 and 76 ± 3.1% of the cultured B16F10 cells. Surprisingly, 32 ± 6% of amelanotic cells (CD9151 and CE9151) produced readable PT signals. Thus, cells defined as amelanotic may produce a small amount of melanin that can be sufficient for their detection using the highly sensitive PT/photoacoustic technique.

As the laser fluence at 850 nm increased, four-phase photoacoustic signal behavior from B16F10 tumor-derived cells was observed (Fig. 2*C*) as follows: (*a*) a gradual increase of linear bipolar photoacoustic signal (left trace) in the range of 10–150 mJ/cm^2; (*b*) nonlinear photoacoustic signal enhancement in the range of 150 to 500 mJ/cm^2 due to bubble formation around overheated melanin nanoparticle clusters (Fig. 2*A, white arrow*), accompanied by a negative peak in the PT thermolens signals as seen in Fig. 2*A* (*bottom row*, *middle*) and photoacoustic signal asymmetry (Fig. 2*C, right trace*); (*c*) saturation (a plateau) of signals in the range of 0.6 to 2 J/cm^2 likely due to laser-induced melanin bleaching of thermal origins; and (*d*) "secondary" nonlinear signal enhancement for fluences of >3 J/cm likely due to thermal explosion of melanin nanoparticles accompanied by shock waves (26). The bubble formation resulted in cell death (13, 17) as confirmed by trypan blue testing. The photodamage threshold ED_{50} (50% cell death after exposure to one laser pulse) was on average 0.39 ± 0.14 J/cm^2, and 0.65 ± 0.19 J/cm^2 and 0.16 ± 0.05 J/cm^2 for low and highly pigmented cells, respectively. The ED_{50} for mouse red blood cells (RBCs) at 850 nm was much higher: 22 ±5.5 J/cm^2. At the same laser energy range in which nonlinear photoacoustic signal amplification from melanoma cells was observed, the photoacoustic signals from RBCs only gradually increased (Fig. 2*C*). Thus, as the laser energy was doubled from 0.2 J/cm^2 to 0.4 J/cm^2, the photoacoustic signals from melanoma cells and RBCs increased ~11 times and approximately twice, respectively, indicating a progressive improvement (~5.5 times) in the detection sensitivity of melanoma cells in the presence of RBCs, and the possibility for inflicting melanoma cell thermal damage without harming the RBCs.

The measured photoacoustic spectra suggest that the preferable spectral ranges providing high photoacoustic contrast of melanoma cells in a background of blood are relatively broad, ranging from 640 to 910 nm (Fig. 3*A*; refs. 9, 27). At 850 nm, the photoacoustic signals from vessels were 3.1 ± 1.1 times higher than the photoacoustic background signals from surrounding tissue. In mice with stronger skin pigmentation, the background photoacoustic signals from ear tissue were 5 ± 1.3 times higher than from nude mouse ears, and thus were a little higher than photoacoustic signals from blood microvessels.

***In vivo* detection of i.v. injected melanoma cells.** Metastatic cells were imitated using ~10^5 B16F10 cells suspended in 100 μL saline solution and injected into the mouse circulatory system through a tail vein followed by their photoacoustic monitoring in an ear vein with a diode laser. To verify that flash photoacoustic signals were from melanoma cells, we periodically used time-resolved two-color OPO mode with pulses at wavelengths of 639 and 865 nm. Because absorption spectra for melanin and venous blood in selected spectral range have distinctive features (decreased and slightly increased absorption with increasing wavelength, respectively; Fig. 3*A*), RBCs generated two permanent photoacoustic signals with higher amplitudes at a wavelength of 865 nm (Fig. 3*B*, *bottom*). In contrast, melanoma cells provided two flash photoacoustic signals with higher amplitudes at a wavelength of 639 nm (Fig. 3*B*, *top*). The number of detected melanoma cells per minute varied for each experiment depending upon the amount of cells introduced into the circulation and the selected vessels. Figure 4*A* shows averaged traces for five animals, and the time points are represented by the mean and SEM. The clearance of melanoma cells was biphasic, including a rapid phase with a rate decrease of approximately four times over 15 to 30 minutes and a much slower phase lasting few hours. In two of the animals, we

observed an increase in the number of CTCs following the initial depletion. This behavior is consistent with previous studies (5, 28) suggesting that arrested CTCs (e.g., in lung or liver) may then release again into the circulation. Melanoma cells labeled *in vitro* before injection with GNRs yielded larger photoacoustic signals above blood background (Fig. 3*A*). The rate of detection for labeled cells was higher than for nonlabeled cells (14.6 ± 1.4 cells/minute versus 12 ± 1.3 cells/minute), thus indicating the capability of PAFC to detect ~82% of melanoma cells in the circulation without labeling. This percentage was lower than in *in vitro* studies (92%), suggesting a false-negative signal rate of 2.6 cells/minute due to background absorption by RBCs. Five-hour monitoring of photoacoustic signals from blood vessels without melanoma cell injection showed no false-positive signals with the signal-to-noise ratio of ≥2. The noise was associated with fluctuation of laser energy and the number of RBCs in the detected volume. After injecting melanin nanoparticles, we observed photoacoustic signals above those of the blood background, which were cleared in ~2 hours (Fig. 4*A*, *bottom*). Both findings are consistent with other data whereby under normal conditions melanin is not present in the blood (2), and clearance of melanin nanoparticles takes longer than the clearance of cancer cells. In mice with high skin pigmentation (Fig. 1*B*, *middle*), the maximum rate of CTC detection was ~10 cells per minute (Fig. 4*A*), indicating an increased false-negative signal rate and the failure to detect ~2 cells per minute.

***In vivo* detection and damage of spontaneous metastatic cells during tumor progression.** PAFC was used to count melanoma CTCs in an ~50-μm-diameter ear blood vessel and an ~150-μm-diameter skin blood vessel during tumor progression in the ear and in skin tumor models (Fig. 4*B*). Scanning of a focused OPO beam (15 μm in diameter) across the tissue near the primary tumor (photoacoustic mapping) revealed in the first week the presence of rare (3–5) local photoacoustic signals within ~1.5 mm of the tumor margin. (Fig. 4*B*). These signals were associated with migration and intravasation of individual melanoma cells or their small aggregates. In some cases, metastatic cells appeared in ear blood microvessels in week 1 without any cells detected in the abdominal skin blood vessels, suggesting that a small amount of adherent CTCs were present in the ear blood vessels while remaining at undetectable levels in the systemic circulation. Two weeks after inoculation, CTCs were detected in the abdominal vessels. This indicates a much greater likelihood of detecting the initial metastatic process in the vicinity of the primary tumor

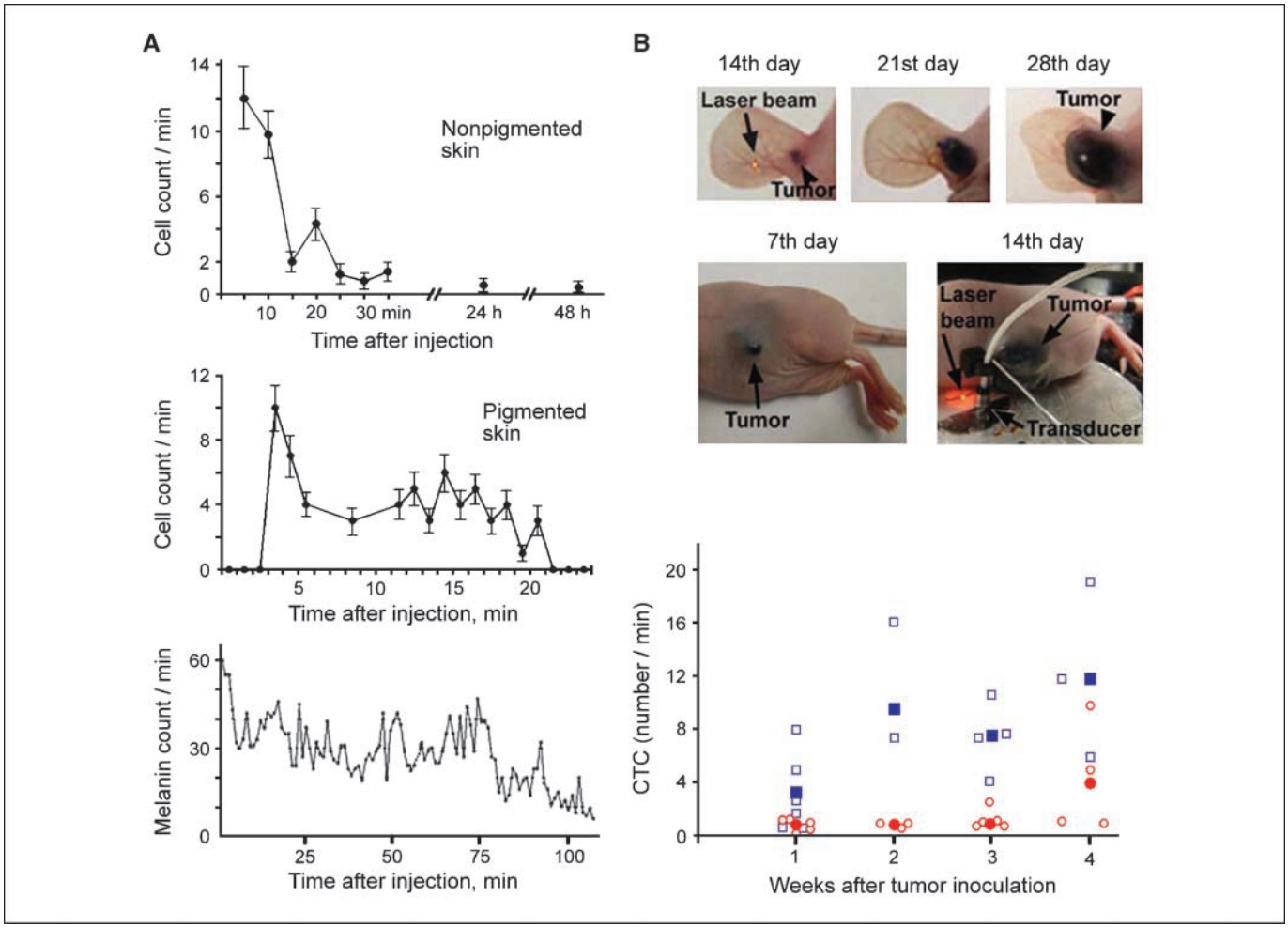

Figure 4. *A*, clearance rate of B16F10 cells in ~50-μm-diameter ear vein in mice with low and high skin melanin pigmentation and 100 nm melanin nanoparticles (2 μg/mL, 50 μL in PBS) as a function of time after injection. Laser parameters: 905 nm, 30 mJ/cm^2. *B*, melanoma tumor growth in mouse ear (*top*) and skin (*middle*) and CTC rate in ~150 μm skin vessels as a function of time after B16F10 tumor cell inoculation in the ear (*red open circle*) and skin (*blue open square*); *filled red circle* and *filled blue square,* averaged data (905 nm, 30 mJ/cm^2).

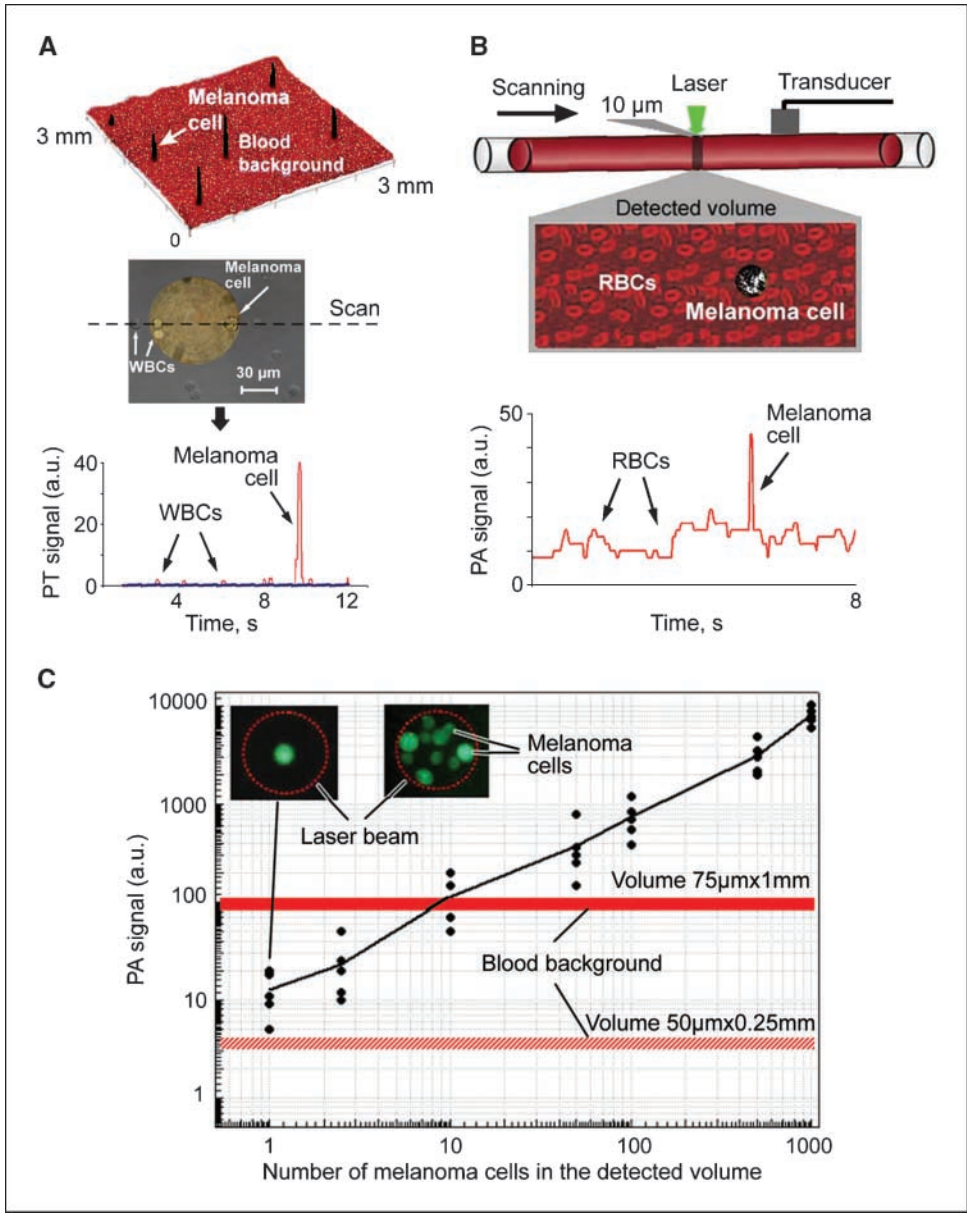

Figure 5. *A,* two-dimensional scanning PT cytometry of single melanoma cells in thin layer (120 μm) of RBCs (*top*), TDM image (*colored central part*) of single melanoma cells among WBCs after RBC lysis (*middle*), and one scan with appearance of one strong PT signal from single melanoma cell in background of low signals from WBCs (850 nm, 100 mJ/cm^2). *B,* one-dimensional scanning photoacoustic capillary cytometry: photoacoustic detection of single B16F10 cells in 0.25-mm diameter of glass tube filled with mouse blood (850 nm, 100 mJ/cm^2). *C,* photoacoustic signals from human blood samples from one donor at different number of melanoma cells in the irradiated volume (850 nm, 150 mJ/cm^2).

before systemic CTC dissemination occurs. The skin tumors grew faster than ear tumors, and skin tumor–born CTCs appeared earlier in the systemic circulation. In particular, by the first week, 1 to 4 CTCs/minute were detected in the skin vasculature, and CTC numbers increased with tumor growth (Fig. 4*B*) up to ~7 CTCs/minute and ~12 CTCs/minute by weeks 3 and 4, respectively. Occasional sequences of photoacoustic signal groups or one photoacoustic signal with a much larger amplitude and elongated width were observed, which support the hypothesis of melanoma cells migrating and circulating as small aggregates (14, 23).

With increased laser energy from 60 to 450 mJ/cm^2 (i.e., nearing CTC photodamage threshold), we observed a decrease in the CTC detection rate from 12 CTC per min to 0.5 to 1 CTC per min following 1 hour of noninvasive exposure to the abdominal skin vessels. In the few days following this procedure, the CTC count nearly returned to the initial levels as new tumor cells entered into the circulation.

A minimally invasive delivery of laser radiation (as proposed in ref. 13) through 100-μm quartz fibers in a tiny needle showed the capability of PAFC to detect CTCs within 200 to 400 μm abdominal skin vessels (Fig. 1*B, right*). This schematic can be used for distinguishing rare individual CTCs with relatively large distances between them (e.g., ≥0.1 mm at concentration ≤10^2 CTC/mL).

The mice were euthanized, and tissue sections from different organs were examined by immunohistochemical staining. The evidence of micrometastasis in sentinel lymph nodes was found starting with week 2–3 for both ear and skin tumor. A gradual increase from rare to multiple micrometastases with dimensions <80 × 60 × 60 μm by weeks 2 to 4 was observed in lung tissue for skin tumor, whereas only a few distant micrometastases were observed by week 4 for ear tumor (Supplementary Fig. S3). Thus, PAFC showed quantitatively that the CTC dissemination rate increased as the tumor progressed, and that CTCs were readily detected weeks before any evidence of metastasis appeared in the tissue samples.

The blood samples (~1.0 mL) were drawn during tumor progression at week 4 and tested by RT-PCR assays (~2.0 mg

extracted total RNA). A slight difference (not statically significant) in Silver gene expression was detected in blood samples (Supplementary Fig. S4), demonstrating the limitation of RT-PCR assays at low CTC concentrations and small sample volumes.

The blood samples collected from mice with tumor were put on slides and scanned with a focused OPO beam (15 μm in diameter). Rare CTCs in blood samples were detected by their remarkable increase in PT signal amplitudes (Fig. 5*A, top*). Melanoma CTCs were verified using TDM to look for specific morphologic features such as cell color associated with melanin, and size greater than normal RBCs (Fig. 2*A, top row, right*). Subsequently, RBCs were lysed and the scanning was repeated without background photoacoustic noise from RBCs (Fig. 5*A, bottom*). Comparison of data *in vivo* and *in vitro* revealed a threshold of PAFC sensitivity of ~1 CTC/mL during 5 hours of monitoring the abdominal vessels. No evidence of metastasis by week 4 was found in mice with skin tumors subjected to daily laser irradiation of the abdominal skin blood vessels (n = 5) for 2 hours at a fluence of 0.7 J/cm^2.

To explore whether melanoma cells can be detected within relatively large vessels against a background of many RBCs, rare B16F10 cells were added to whole blood samples from normal mice and placed in glass tubes with inner diameters of 0.25 mm, followed by continuous scanning of the tubes using a focused laser beam. During photoacoustic scanning, rare and strong photoacoustic signals were occasionally observed against a background of lower photoacoustic signals from RBCs (Fig. 5*B, bottom*).

Next, cultured human melanoma cells (HTB-65) were added to anticoagulated blood samples from healthy human donors and subjected to PAFC in microscopic chambers of varying concentrations of melanoma cells (~1, 3, 10, 50, 100, 500, and 1,000 cells per unit of volume analyzed). The average numbers of melanoma cells and RBCs were verified by TDM using thin slides and fluorescent imaging by staining melanoma cells with FITC. This study revealed a detection limit at a signal-to-noise ratio of 2 of one melanoma cell in the irradiated volume (beam diameter of 50 μm × sample thickness of 0.25 mm; Fig. 5*C*). For a larger irradiated volume (beam diameter of 75 μm × sample thickness of 1 mm), the detection limit was a minimum of 10 to 20 CTCs. *In vivo* irradiation of a peripheral blood vessel, through layers of animal skin covering the intact skin, showed the ability of PAFC to assess vessels with an unfocused transducer at a depth of 4 mm at 532 nm (Supplementary Fig. S5) and potentially deeper in the NIR range (6). The measurement of melanoma CTC rates using the ear tumor model at week 4 with a nonfocused transducer on a 50-μm ear vessels and 150-μm skin vessels revealed CTC rates of 0.06 and 4.0 CTCs/minute, respectively. The measurements using focused transducer of a ~0.9 mm aorta (Supplementary Fig. S5) revealed a CTC rate of 71 CTCs/minute. This study shows a higher probability of detecting CTCs using a focused transducer on large deep vessels with higher flow allowing circulation of almost the entire mouse's blood volume (~2 mL) within 0.5 to 1 min (20).

The improvement of PAFC's capability. We have identified several methods for improving PAFC sensitivity. Because deoxygenated (Hb) and oxygenated (HbO_2) hemoglobin absorbs differently (27), the change in blood oxygenation from norm (e.g., ~75% in vein; ref. 27) may lead to decreased total blood absorption. Indeed, increased oxygenation by pure oxygen delivery during 15 minutes using a mask around a mouse's head caused a 1.36 ± 0.14-fold signal decrease from veins at a wavelength of 750 nm. Decreasing the hematocrit is another way to decrease photoacoustic background signals due to a decrease in numbers of RBCs in the detected volume. After injection of 0.5 mL standard saline solution (20–25% dilation that is within physiologic norm in human; refs. 22, 27) into a tail vein, background photoacoustic signals from a 50-μm mouse ear vein were immediately decreased 2.3 ± 0.3-fold. Osmolarity causes an increase in the RBC volume through swelling (27) that may result in a decrease the photoacoustic signals. Indeed, the injection of 100 μL hypertonic solution of NaCl into the mouse tail vein led to a drop in the photoacoustic signal in the ear vein by ~2-fold, correlated with an RBC size increase monitored by TDM.

A decrease in the lumen diameter of blood microvessels to 10 to 15 μm through gentle mechanical occlusion for 10 min (Fig. 6), followed by the quick release of the vessel led to an immediate increase in the rate of metastatic melanoma cells by ~3-fold. It is likely that melanoma cells with typical sizes of 15 to 25 μm were trapped, and thus concentrated at the entrance of the vessel bottleneck, whereas smaller RBCs (5–6 μm) and leukocytes (7–8 μm; refs. 20, 21) continued to traverse the portion of the vessel lumen with a reduced diameter.

Discussion

The label-free nature of PAFC using melanin as an intrinsic cell marker offers avoidance of potential problems related to labeling of CTCs *in vivo* (7, 29–32). This may provide the precedent for noninvasive, *in vivo* blood cancer testing that focuses on melanoma, a highly aggressive, epidemic malignancy that is often

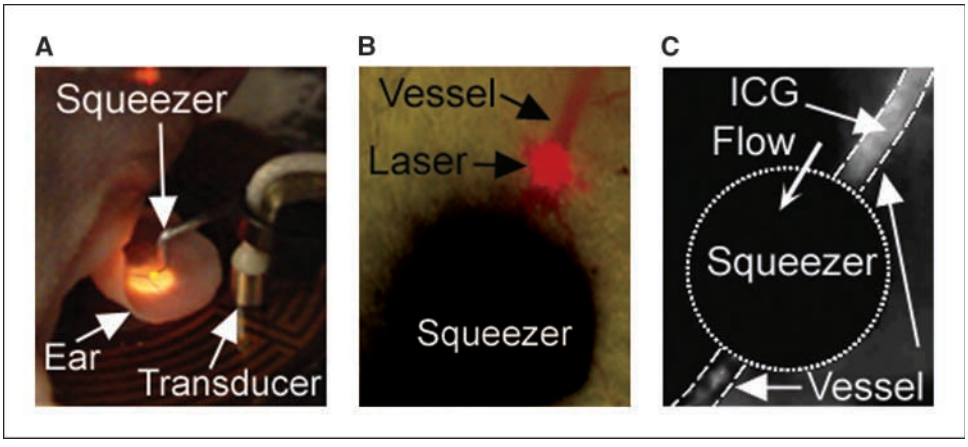

Figure 6. *A, in vivo* capturing of relatively large CTCs and their clusters by gentle mechanical squeezing of the blood vessel in mouse ear. *B,* image of a blood vessel area during squeezing with a pilot red (633 nm) laser beam. *C,* fluorescent control of squeezing (excitation with diode laser, 805 nm, 0.5 W; emission, 830 nm) showing the accumulation of i.v. (injected in tail vein) Indocyanine Green (*ICG*) dye in blood vessel before the area is squeezed (*top, right*) and a decrease in the Indocyanine Green concentration after the area is squeezed (*bottom, left*).

widely metastatic at an early stage (33, 34). The threshold sensitivity of 1 CTC/mL achieved in our experiments was primarily limited by the small blood volume (~2 mL) present in mice and realistic monitoring times, rather than by PAFC parameters. According to our data, PAFC is capable of detecting a single CTC in the presence of $\sim 10^3$ RBCs in the irradiated volume at 850 nm, suggesting a high absorption contrast of melanin when compared with hemoglobin in the NIR range (12, 17, 35, 36). In superficial capillaries, CTCs can be detected with a high optical resolution (5–15 μm) without interference from RBCs, which flow single-file through the vessels (6); however, large CTCs are less plentiful in these small vessels with slow flow rate. To minimize the detection volume in deeper vessels with stronger light scattering, a focused cylindrical ultrasound transducer can be used with a high lateral acoustic resolution (~100 μm at 20 MHz), and an axial resolution comparable with the cross-section of the irradiated vessel.

According to ours and other data (5–7), the sensitivity versus time-of-observation thresholds can be roughly estimated as the following: in 50-μm vessels, 1 CTC/1 mL in ~5 to 10 hours; in 100 to 300 μm vessels, 1 CTC/10 mL in ~1 hour; in 1 to 3 mm hand vein at ~3 mm depth, 1 CTC/100 mL in ~1 hour; and in 10 to 15 mm human jugular vein at a depth of 15 to 20 mm (37), 1 CTC/(3–5 liters) in 5 to 10 minutes. Thus, hypothetically, photoacoustic blood monitoring in a large vessel during just 10 minutes can improve CTC detection sensitivity by 10^2- to 10^3-fold compared with existing assays (≥ 1 CTC/mL).

Approximately 18% as in the current study and potentially more of CTCs with low melanin expression can be missed with label-free PAFC. Nevertheless, this level is still less than or comparable with conventional assays, which can miss up to 30% to 70% of CTCs due to the limited expression of biomarkers used for targeting of cancer cells (e.g., folate receptors or HER2; refs. 7, 38). Further improvements in the signal-to-noise ratios can be achieved by enhancing melanin synthesis using drugs (Supplementary Fig. S6) or other melanin activators (39), "clearance" of NIR window transparency through alteration of blood parameters, capturing of large CTCs by squeezing small vessels or putting "nets" into vessels, better matching of the laser pulse width with the acoustic and thermal relaxation times of melanin nanoparticles (40, 41), use exogenous strongly absorbing low-toxic labels (e.g., gold nanoparticles; ref. 6), and laser-induced clustering of nanoparticles (42). Melanin-containing (or engineered) pathogens (e.g., Salmonella) could be also used as potential vectors for targeting low-pigmented metastases (43, 44).

PAFC may fill the gaps in cutaneous and uveal (45) melanoma research with a focus on label-free monitoring (free of toxicity concerns) of cancer cell intravasation and blood/lymph dissemination in various microenvironments, *in vivo* study of melanin synthesis at the subcellular level, and a putative link between melanin expression and metastatic potential of CTCs (through comparison of photoacoustic signals from cells in primary tumor, CTCs, and distant metastases). Clinical scenarios may include the following: (*a*) blood screening for early CTCs before development of metastasis; (*b*) testing for cancer recurrence; (*c*) individualized assessment of therapeutic efficacy through real-time CTC count; (*d*) detection of cancer cells around surgical sites (to evaluate margins for residual cancer cells); and (*e*) inhibition of the development of metastases and potentially their prevention by well-timed laser blood purging. Further study could determine whether this new treatment is effective enough to be used alone or if it should be used in conjunction with chemotherapy and radiation therapy. Taking into account successful clinical applications of photoacoustic techniques (8, 37) and the safe range of laser fluence (20–35 mJ/cm^2) required, which is within the laser safety standard for human use (20–100 mJ/cm^2 at wavelengths of 500 nm–1100 nm; ref. 46), we anticipate quick translation of PAFC technology in humans using a portable device composed of a high pulse rate diode laser array with different wavelengths under guidance of ultrasound or NIR imaging techniques (Supplementary Fig. S7; ref. 47).

Disclosure of Potential Conflicts of Interest

No potential conflicts of interest were disclosed.

Acknowledgments

Received 12/30/08; revised 8/4/09; accepted 8/5/09; published OnlineFirst 10/13/09.

Grant support: NIH grants R01 EB000873, R01 CA131164, R01 EB009230, R21 CA139373, and the National Science Foundation grant DBI 0852737 and by the Arkansas Bioscience Institute.

The costs of publication of this article were defrayed in part by the payment of page charges. This article must therefore be hereby marked *advertisement* in accordance with 18 U.S.C. Section 1734 solely to indicate this fact.

We thank Xiao-Dong Chen for providing mice with strong skin pigmentation, Leah Henning for pathologic examination, Williams Tolleson for providing RT-PCR analysis and amelanotic cells, Yaroslav Simanovsky for the initial study with a diode laser, Dmitry Lapotko for help with PT microscope, Scott Ferguson for his assistance with laser measurements, and Sherry Holmen for providing data for drug-induced melanoma cell pigmentation.

References

1. Abbot A. The root of the problem. Nature 2006;442:742–3.
2. Mocellin S, Hoon D, Ambrosi A, Nitti D, Rossi CR. The prognostic value of circulating tumor cells in patients with melanoma: a systematic review and meta-analysis. Clin Cancer Res 2006;12:4605–13.
3. Nagrath S, Sequist LV, Maheswaran S, et al. Isolation of rare circulating tumor cells in cancer patients by microchip technology. Nature 2007;450:1235–9.
4. Riethdorf S, Fritsche H, Müller V, et al. Detection of circulating tumor cells in peripheral blood of patients with metastatic breast cancer: a validation study of the CellSearch system. Clin Cancer Res 2007;13:920–8.
5. Georgakoudi I, Solban N, Novak J, et al. *In vivo* flow cytometry: a new method for enumerating circulating cancer cells. Cancer Res 2004;64:5044–7.
6. Zharov VP, Galanzha EI, Shashkov EV, Khlebtsov NG, Tuchin VV. *In vivo* photoacoustic flow cytometry for monitoring of circulating single cancer cells and contrast agents. Opt Lett 2006;31:3623–5.
7. He W, Wang H, Hartmann LC, Cheng JX, Low PS. *In vivo* quantitation of rare circulating tumor cells by multiphoton intravital flow cytometry. Proc Natl Acad Sci U S A 2007;104:11760–5.
8. Xu M, Wang LV. Photoacoustic imaging in biomedicine. Rev Sci Instrum 2006;77:041101.
9. Zhang HF, Maslov K, Stoica G, Wang LV. Functional photoacoustic microscopy for high-resolution and noninvasive *in vivo* imaging. Nat Biotechnol 2006;24:848–51.
10. Zerda A, Zavaleta C, Keren S,et al. Carbon nanotubes as photoacoustic molecular imaging agents in living mice. Nat Nanotechnol 2008;3:557–62.
11. Weight RM, Viator JA, Dale PS, Caldwell CW, Lisle AE. Photoacoustic detection of metastatic melanoma cells in the human circulatory. Opt Lett 2006;31:2998–3000.
12. Ara G, Anderson RR, Mandel KG, Ottesen M, Oseroff AR. Irradiation of pigmented melanoma cells with high intensity pulsed radiation generates acoustic waves and kills cells. Lasers Surg Med 1990;10:52–9.
13. Zharov VP, Galanzha EI, Shashkov EV, et al. Photoacoustic flow cytometry: principle and application for real-time detection of circulating single nanoparticles, pathogens, and contrast dyes *in vivo*. J Biomed Opt 2007;12:051503.
14. Galanzha EI, Shashkov EV, Tuchin VV, Zharov VP. *In vivo* multiparameter, multispectral lymph flow cytometry with natural cell focusing, label-free detection and multicolor nanoparticle probes. Cytometry A 2008;73A:884–94.
15. Tolleson WH. Human melanocyte biology, toxicology, and pathology. J Environ Sci Health C Environ Carcinog Ecotoxicol Rev 2005;23:105–61.

16. Alekseeva AV, Bogatyrev VA, Dykman LA, et al. Preparation and optical scattering characterization of Au nanorods, and their application to a dot-immunogold assay. Appl Opt 2005;44:6285–95.
17. Zharov VP, Lapotko DO. Photothermal imaging of nanoparticles and cells. IEEE J Sel Topics Quant Electron 2005;11:733–51.
18. Zharov VP, Galanzha EI, Tuchin VV. Photothermal flow cytometry *in vitro* for detection and imaging of individual moving live cells. Cytometry A 2007;71A: 191–206.
19. Zharov VP, Galanzha EI, Tuchin VV. *In vivo* photothermal flow cytometry: imaging and detection of cells in blood and lymph flow. J Cell Biochem 2006;97: 916–32.
20. Charm SE, Kurland GS. Blood flow and microcirculation. John Wiley & Sons; 1974.
21. Schmidt RF, Thews G, editors. Human Physiology. Berlin, Heidelberg, New York, London, Paris, Tokyo, Hong Kong: Springer-Verlag; 1989.
22. Halaban R. Pigmentation in melanomas: changes manifesting underlying oncogenic and metabolic activities. Oncol Res 2002;13:3–8.
23. Ishikawa M, Fernandez B, Kerbel RS. Highly pigmented human melanoma variant which metastasizes widely in nude mice, including to skin and brain. Cancer Res 1988;48:4897–903.
24. Gray-Schopfer V, Wellbrock C, Marais R. Melanoma biology and new targeted therapy. Nature 2007;445: 851–7.
25. Schatton T, Murphy GF, Frank NY, et al. Identification of cells initiating human melanomas. Nature 2008;451: 345–9.
26. Pustovalov V, Smetannikov A, Zharov V. Photothermal and accompanied phenomena during selective nanophotothermolysis with absorbing nanoparticles and pulse lasers. Laser Phys Lett 2008;5:775–92.
27. Roggan M, Friebel K, Dorschel H, Andreas H, Muller G. Optical properties of circulating human blood in the wavelength range 400-2500 nm. J Biomed Opt 1999;4: 36–6.
28. Fidler I. Metastasis: quantitative analysis of distribution and fate of tumor emboli labeled with ^{125}I-5-Iodo-2′-deoxyuridine. J Natl Cancer Inst 1970;45:773–82.
29. Novak J, Georgakoudi I, Wei X, Prossin A, Lin CP. *In vivo* flow cytometer for real-time detection and quantification of circulating cells. Opt Lett 2004;29:77–9.
30. Nolte MA, Kraal G, Mebius RE. Effects of fluorescent and nonfluorescent tracing methods on lymphocyte migration *in vivo*. Cytometry A 2004;61:35–44.
31. Wei X, Runnels JM, Lin CP. Selective uptake of indocyanine green by reticulocytes in circulation. Invest Ophthalmol Vis Sci 2003;44:4489–96.
32. Abbitt KB, Rainger GE, Nash GB. Effects of fluorescent dyes on selectin and integrin-mediated stages of adhesion and migration of flowing leukocytes. J Immunol Methods 2000;239:109–19.
33. Linos E, Swetter SM, Cockburn MG, Colditz GA, Clarke CA. Increasing burden of melanoma in the United States. J Invest Dermatol 2009;129:1666–74.
34. Weinstock MA. Cutaneous melanoma: public health approach to early detection. Dermatol Ther 2006;19: 26–31.
35. Lin CP, Kelly MW, Sibayan SAB, Latina MA, Anderson RR. Selective cell killing by microparticle absorption of pulsed laser radiation. IEEE Selected topics in Quantum Electronic 1999;5:963–7.
36. Dees C, Harkins J, Petersen MG, Fisher WG, Wachter EA. Treatment of murine cutaneous melanoma with near infrared light. Photochem Photobiol 2002;75:296–301.
37. Petrov YY, Petrova IY, Patrikeev IA, Esenaliev RO, Prough DS. Multiwavelength optoacoustic system for noninvasive monitoring of cerebral venous oxygenation: a pilot clinical test in the internal jugular vein. Opt Lett 2006;31:1827–9.
38. Ludwig JA, Weinstein JN. Biomarkers in cancer staging, prognosis and treatment selection. Nat Rev Cancer 2005;5:845–56.
39. Koo HM, VanBrocklin M, McWilliams MJ, et al. Apoptosis and melanogenesis in human melanoma cells induced by anthrax lethal factor inactivation of mitogen-activated protein kinase. Proc Natl Acad Sci U S A 2002;101:10501–4.
40. Zharov VP, Kim J-W, Everts M, Curiel DT. Self-assembling nanoclusters in living systems: application for integrated photothermal nanodiagnostics and nanotherapy. Nanomedicine 2005;1:326–45.
41. Shashkov E, Everts M, Galanzha E, Zharov V. Quantum dots as multimodal photoacoustic and photothermal contrast agents. Nano Lett 2008;8:3953–8.
42. Zharov VP, Galitovskaya EN, Jonson C, Kelly T. Synergistic enhancement of selective nanophotothermolysis with gold nanoclusters: potential for cancer therapy. Laser Surg Med 2005;37:219–26.
43. Plonka PM, Grabacka M. Melanin synthesis in microorganisms-biotechnological and medical aspects. Acta Biochim Pol 2006;53:429–43.
44. Jia LJ, Wei DP, Sun QM, Huang Y, Wu Q, Hua ZC. Oral delivery of tumor-targeting Salmonella for cancer therapy in murine tumor models. Cancer Sci 2007;98: 1107–12.
45. Callejo SA, Antecka E, Blanco PL, Edelstein C, Burnier MN, Jr. Identification of circulating malignant cells and its correlation with prognostic factors and treatment in uveal melanoma. A prospective longitudinal study. Eye 2007;21:752–9.
46. American National Standard for safe use of lasers. ANSI Z136 2000;1.
47. Zharov VP, Ferguson S, Eidt JF, et al. Infrared imaging of subcutaneous veins. Laser Surg Med 2004;34:56–61.